Resonant Acoustic Frequency Shifts Associated with Cracks in Multilayer Ceramic Capacitors

Ward L. Johnson, Jaemi L. Herzberger, Sudook A. Kim, Kirsten L. Peterson, Paul R. Heyliger, and Grady S. White

Abstract—**Resonant ultrasound spectroscopy (RUS) was used in this study to measure shifts in resonant frequency that arise from the presence of cracks in barium-titanate-based multi-layer ceramic capacitors (MLCCs). This work was motivated by an industrial need for a nondestructive quality-control technique with enhanced capabilities for detecting dielectric cracks that have no initial effect on electrical characteristics of MLCCs. In this quality-control application, no information will generally be available on acoustic spectra of capacitors prior to the introduction of cracks during manufacture or mounting in devices. However, information on the distribution of frequencies of a specified resonant acoustic mode of a population of uncracked MLCCs could serve as a reference for determining whether the resonant frequency of an individual MLCC is within an acceptable range. In this study, acoustic spectra were obtained from sets of MLCCs before and after thermal quenching that generated surface-breaking cracks in a fraction of the specimens. Three resonant modes below 1000 kHz were studied. The largest of these three resonant peaks, in the range of 575 kHz to 595 kHz in MLCCs before heat treatment, was found to be most sensitive to the presence of visible cracks. An analysis of Gaussian fits of the frequency distributions for this mode before and after heat treatment shows that approximately 71 % of the visibly cracked MLCCs and less than 1 % of the uncracked quenched MLCCs are rejected when the criterion for rejection is that the frequency is more than two standard deviations different than the mean frequency before heat treatment. These results show that RUS is a promising approach for nondestructive screening for the presence of cracks in MLCCs.**

I. Introduction

Multilayer ceramic capacitors (MLCCs) are widely employed in electronic circuits because of their high capacitance and small dimensions. However, failure of MLCCs can be a limiting factor in the reliability of electronic devices in which they are incorporated [1]. Capacitor failure is of particular concern in high-end applications where device failure can be catastrophic and/or repair can be costly or dangerous, such as medical implants and space applications. The great number of MLCCs employed in some electronic systems also makes the requirements for reliability much more challenging. For example, some space hardware assemblies contain thousands of MLCCs [2].

The dominant failure mechanism in MLCCs is cracking of the brittle dielectric, which occurs due to mechanical stress during manufacture, installation, and/or operation. Thermal shock and board flexure are two leading causes of dielectric cracks [1]. The solder reflow process that is used to attach MLCCs to boards can produce thermal-shock in an MLCC, governed by the temperature stability and fracture toughness of the dielectric [2]. Additionally, post-soldering handling of a printed circuit board (PCB) on which an MLCC is mounted can lead to excessive flexure that generates cracks in the ceramic dielectric [3]. These cracks are typically microscopic, initially, and do not lead to an immediate detectable effect on the electrical characteristics of the capacitor. Rather, electrical failures occur when environmental factors cause electrochemical migration and associated shorting [4] or external stresses cause a crack to propagate through the electrodes, creating an electrical open.

The limitations of screening methods such as electrical leakage testing and visual inspection [2], [5], [6] have led to an exploration of acoustic techniques that could provide the basis for inspection systems for nondestructively sensing dielectric cracks in industrial settings. This research has included resonant laser ultrasonics, scanning acoustic microcopy, electromechanical resonance, resonant ultrasound spectroscopy (RUS), and nonlinear resonant acoustics [5]–[14]. The principal focus on resonant methods in these prior studies arises partly from the fact that the most likely areas for cracking of MLCCs during manufacture and device fabrication are the ceramic regions beneath the endcaps, which are not readily accessible to localized acoustic scanning techniques. Our previous research on methods for sensing cracks in MLCCs included nonlinear resonance measurements with tone-burst ferroelectric excitation and found a strong correlation of the amplitude dependence of frequencies with the presence of visible cracks in thermally stressed (quenched) specimens [13], [14]. We also previously employed RUS to study resonant frequency shifts in MLCCs subjected to thermal shock, microindentation, elevated vibration/temperature/current, and a linear flaw produced by focused-ion-beam (FIB) milling. In that RUS study, accelerated stress and thermal shock were found to induce the most significant shifts in frequencies, although the sign of these shifts varied. The present report describes a more extensive study of the effects of cracks on RUS frequencies of free-

W. Johnson, S. Kim, and G. White are with the National Institute of Standards and Technology, Applied Chemicals and Materials Division, 325 Broadway St., Boulder, CO 80305. e-mail: ward.johnson@nist.gov.

J. Herzberger was with NASA Goddard Space Flight Center (GSFC), Greenbelt, MD 20771 and University of Maryland, College Park, MD 20742.

K. Peterson and P. Heyliger are with Colorado State University, Dept. of Civil and Environmental Engineering, Colorado State University, Fort Collins, CO 80523

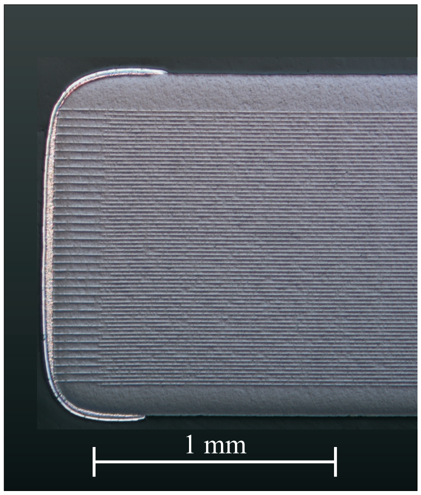

Fig. 1. Half of a cross section of an MLCC showing the 70 internal Ag electrodes interleaved with dielectric and one of the endcaps.

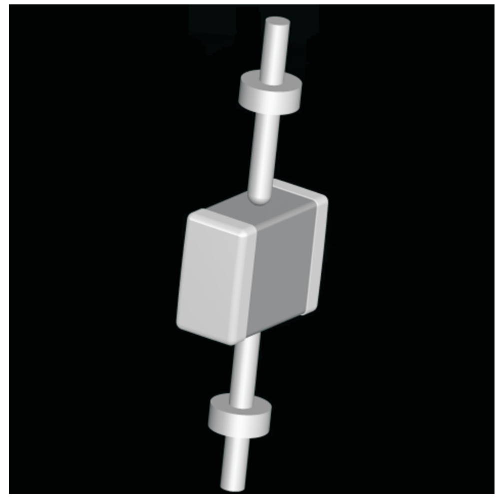

Fig. 2. RUS configuration with contact of transducers (top and bottom) for excitation and detection on opposite small ceramic faces of the specimen (middle). Interior electrode layers are parallel to the large faces of the specimen.

standing MLCCs subjected to thermal quenching and presents a brief comparison of RUS results with previous nonlinear tone-burst results for similarly quenched capacitors.

II. Specimens

The specimens in this study are type-1210 MLCCs manufactured by Vishay Intertechnology, with model number VJ1210Y474KXAAT.[1] Figure 1 shows a partial cross section of a specimen. The MLCC is comprised of a doped barium titanate ($BaTiO_3$) dielectric with X7R (Electronic Industries Alliance standard) performance specification and 70 interleaving silver (Ag) electrodes. Additionally, a nickel (Ni) diffusion-blocking layer is located between a pool of Ag and an outer tin (Sn) solder termination layer on both ends of the MLCC. Measurements of the geometry of a set of capacitors representative of the specimens in this study are presented elsewhere [13]. The overall dimensions of the ceramic (not including metal endcaps) are (1.40 $\pm$ 0.02) mm, (3.04 $\pm$ 0.01) mm, and (2.46 $\pm$ 0.01) mm, with the indicated uncertainties being standard deviations of measurements on seven MLCCs. The core electrodes were found to have a thickness of (2.0 $\pm$ 0.2) μm and an average periodicity of (16.38 $\pm$ 0.05) μm.

III. Methods

A. Acoustic measurements

Resonant ultrasound spectroscopy (RUS) employs narrowband excitation and detection with the frequency incremented in steps over a specified frequency range, leading to acquisition of resonant spectra. RUS has previously been employed in many studies to determine elastic-stiffness coefficients from measured resonant frequencies and has been shown to be sensitive to the presence of cracks and other material defects [15], [16]. RUS employs a piezoelectric transducer, driven by a sinusoidal voltage from a frequency synthesizer and in contact with a small area of the specimen, to excite vibrations in the specimen at the excitation frequency. A second piezoelectric transducer in contact with another region of the surface of the specimen (typically on the opposite side of the specimen) senses the amplitude of vibrations. The signal from the second transducer is passed to a lock-in amplifier that employs the synthesizer output as a reference. To obtain a resonance spectrum of a specimen, the synthesizer frequency is stepped through the range of interest, and peaks appear at excitation frequencies that match those of the acoustic normal modes. The dwell time at each frequency is set to a value substantially greater than the exponential decay time of the resonant modes to avoid skewing of peaks [15].

In this study, a configuration with flat-faced piezoelectric transducers making contact on opposite diagonal corners of a specimen was found to provide resonant spectra with so many closely spaced peaks that useful information could not be extracted from the spectra. Much of the complexity of these spectra is interpreted as arising from spurious resonances within the transducers themselves, the magnitude of which is affected by the strength of coupling to a specimen. Spectra with fewer peaks were obtained through the use of piezoelectric transducers with hemispherical wear plates pressed against opposite flat surfaces of a specimen. Figure 2 shows the final configuration that was employed, with the excitation and sensing transducers making contact with the small ceramic faces of an MLCC. As discussed below, spectra obtained with this setup still show evidence for excitation of transducer resonances at modest levels, so that additional steps must be taken in spectral analysis.

Uncertainties in measured resonant frequencies were determined by repeatedly acquiring spectra with a specimen removed from and, then, reinserted between the transducers after

[1] Identification of this commercial product is provided for technical completeness and does not reflect an endorsement by NIST.

TABLE I
NUMBER OF SPECIMENS AND HEAT-TREATMENT TEMPERATURES FOR THE ELEVEN GROUPS OF MLCCS.

Group index	Number of specimens	HT Temp. (°C)
1	10	181
2	10	203
3	10	197
4	10	202
5	7	187
6	7	203
7	5	214
8	6	140
9	10	204
10	10	202
11	10	203

each spectrum. Twenty-seven spectra were included in this sequence, and standard deviations of the measured frequencies of each peak were determined from these spectra.

B. *Heat treatments*

Each of the eleven groups of specimens was placed on a stainless steel tray and inserted into a box furnace at a temperature above the phase-transition temperature of barium titanate ($\sim$ 125 °C), where the crystal structure changes from cubic to tetragonal crystal structure on cooling. Each group was left in the furnace for approximately 5 minutes and, then, removed from the furnace and immediately quenched by dropping into ice water. The set temperature of the furnace for each group, in addition to the number of specimens in the group, are listed in Table I. The heat-treatment temperatures of the groups were varied over the course of the study, with the aim of varying the number of specimens that were cracked by the heat treatment. As described below, no significant correlation was found between resonant frequencies in cracked specimens and the heat-treatment temperatures of these specimens.

C. *Optical inspection*

A modified version of the "vicinal illumination" technique of Burns and Yang [17] was employed to detect cracks generated by heat treatment. The specific procedure described by Burns and Yang could not be employed with the required magnifications (greater than 20X), because the space between the specimen and the objective lens in a microscope was too small to insert external lights. The technique was modified by reducing the field diaphragm of the microscope, or partially rotating the incident light reflector turret from the bright field settings, to produce nonuniform lighting. The outer edge of the field diaphragm, or outer shaded boundary from the partially rotated incident light reflector turret, was visually searched for cracks. No cracks were detected in any of the MLCCs before heat treatment.

D. *Finite element calculations*

Theoretical values of the resonant frequencies were computed using the finite element method. This technique is well established in giving excellent approximations for both the frequency spectrum and the displacement patterns associated with each mode. These are computed through the use of piecewise approximations to the three displacement components combined with the weak form of the equations of motion, as expressed by Hamilton's Principle [18]. The discretized form of these approximations results in the standard eigenvalue equation, given by

$$[K]\{u\} = \omega^2[M]\{u\}, \tag{1}$$

where the matrix $[K]$ contains the terms associated with strain energy, $[M]$ contains the terms associated with kinetic energy, ω is the natural angular frequency of vibration, and $\{\mathrm{u}\}$ contains the modal displacement vector. A number of symmetry arguments can be made to reduce the size of this eigenvalue problem according to the nature of the modal displacements, and it is possible to reduce the physical domain and associated boundary conditions into eight separate problems involving a single octant of the actual physical geometry. Details of this procedure are given elsewhere [19].

IV. RESULTS

A. *Principal spectral peaks*

Figure 3 shows typical resonance spectra, with frequency-independent backgrounds subtracted, obtained from an as-received (AR) capacitor before heat treatment (without visible cracks) and after heat treatment (HT). The capacitor from which these spectra were obtained had visible cracks after heat treatment. The largest peak is near 582 kHz in the AR spectrum and near 572 kHz in the HT spectrum. Additional peaks appear in the ranges of 450 kHz to 480 kHz and 970 kHz to 1200 kHz. A peak in the range of at 590 kHz to 610 kHz is present on the high-frequency shoulder of the main peak before and after heat treatment, and similar small peaks are visible on the shoulders of the other peaks.

Figure 4 shows the same two spectra over a narrower frequency range near 600 kHz. The main peak is shifted substantially downwards in frequency (by approximately 10 kHz), and the shift in the smaller peak, if any, is much less. This general behavior was found to be typical of spectra from AR and cracked HT specimens in this study.

Finite element (FE) calculations predict that, in the frequency range of Fig. 4, there is only one acoustic resonance, with a frequency of approximately 590 kHz [19]. This mode in the FE calculations is nondegenerate, as are all normal modes in objects with orthorhombic or lower symmetry [20]. Therefore, the presence of the second peak in Fig. 4 cannot be explained by degenerate-mode splitting arising from a deviation from exact orthorhombic symmetry.

The possibility that the smaller peak in Fig. 4 is not an acoustic resonance of the specimen was explored by performing RUS measurements with the excitation and detection transducers directly touching one another (without a specimen present). A spectrum obtained over the frequency range of 550 kHz to 650 kHz in this configuration shows a peak with a maximum at (601 $\pm$ 5) kHz. This result is consistent with the weaker peak in the range of 595 kHz to 598 kHz in Fig. 4

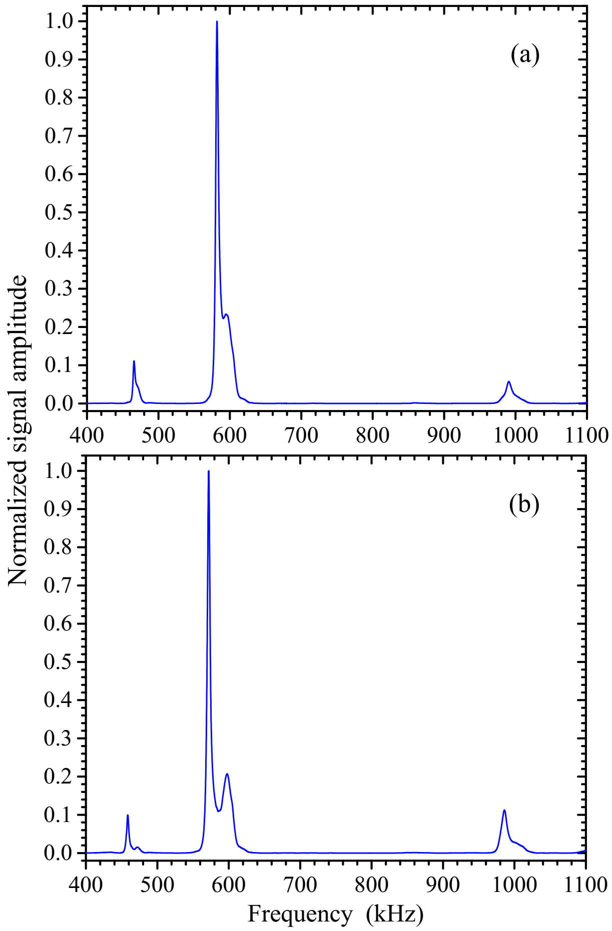

Fig. 3. RUS spectra of a capacitor (a) before and (b) after quenching from 197 °C (Group 3), normalized to the height of the largest spectral peak in each spectrum. Before heat treatment, no cracks were seen in an optical microscope. After heat treatment, the capacitor was determined from optical inspection to have cracks at the surface of the ceramic.

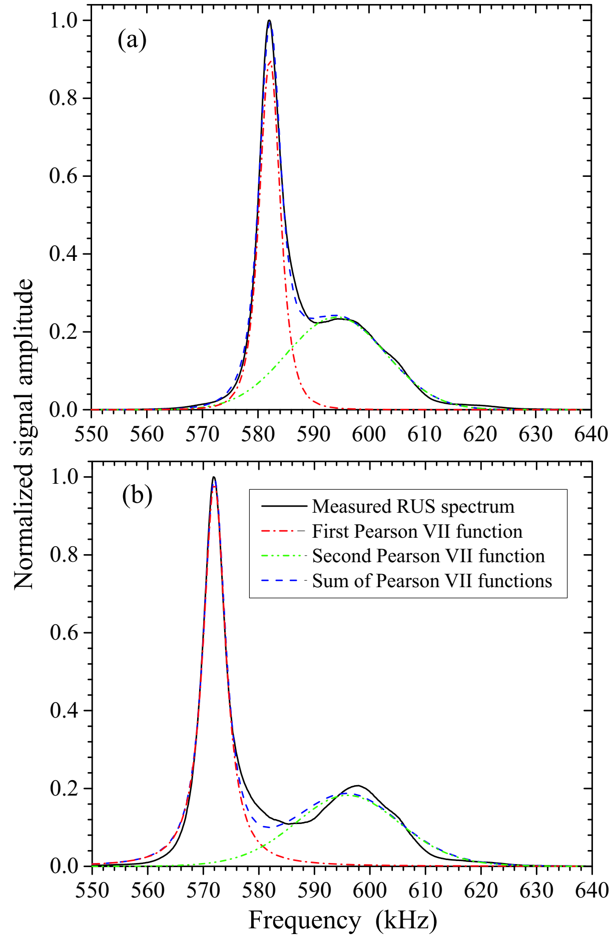

Fig. 4. Spectra of Fig. 3 over a narrower frequency range of 550 kHz to 640 kHz and fits of these data to the sum of two Pearson VII functions: (a) before quenching and (b) after quenching from 197 ∘C.

being an instrumental artifact arising from resonances of one or both of the transducers. This conclusion is further supported by the fact that analysis of additional spectra acquired from all of the MLCCs in this study showed no significant correlation of the frequencies of the smaller peak (closest to 600 kHz) with the presence of cracks.

A similar situation exists with the small peaks that appear on the shoulders of the main peaks in the ranges of 450 kHz to 480 kHz and 970 kHz to 1200 kHz in Fig. 3. A spectrum over the range of 400 kHz to 1100 kHz (not shown) obtained with transducers directly touching one another contains, in addition to the strong peak near 601 kHz, smaller peaks at (420 $\pm$ 2) kHz, (476 $\pm$ 2) kHz, (519 $\pm$ 3) kHz (870 $\pm$ 5) kHz, (945 $\pm$ 5) kHz, (1003 $\pm$ 5) kHz, and (1083 $\pm$ 5) kHz. The peaks measured in this configuration near 476 kHz and 1003 kHz are within a few kilohertz of shoulder peaks in Fig.3(b), consistent with the hypothesis that these peaks in the spectra from MLCCs are transducer resonances. As with the peak near 600 kHz in MLCC spectra, these shoulder peaks near 476 kHz and 1003 kHz were not found to be significantly correlated with the presence of cracks in the capacitors.

The graphs in Fig. 4 include fits of each measured spectrum to a superposition of two Pearson VII spectroscopic functions over the 550 kHz to 640 kHz range. The Pearson VII function [21] (which is symmetric) includes an adjustable parameter that provides peak shapes between that of a Lorentzian and a Gaussian and, thus, fits the main peak more closely than either of these simpler functions. However, the second (smaller) Pearson VII function does not provide a close match to the shape and maximum of the minor peak (near 598 kHz), and this is most obvious in the heat-treated spectrum (Fig. 4(a)), where the peaks are more clearly separated. Since this peak was determined to be an instrumental artifact and is not considered in further analysis of the spectra, the use of a more complicated fitting function to match this peak (for example, including additional Pearson VII functions in the sum) was considered to be unwarranted.

Finite-element calculations over the frequency range from 0 kHz to 1000 kHz predict normal-mode frequencies at approximately 354 kHz, 474 kHz, 590 kHz, 657 kHz, 691 kHz, 701 kHz, 709 kHz, 772 kHz, 803 kHz, 848 kHz, 862 kHz, 876 generally not be available for individual capacitors before they are exposed to stresses that potentially generate cracks, but measurements could be performed to determine the mean and standard deviation of frequencies of a population of uncracked and cracked capacitors with the same nominal specifications, materials, and processing parameters as those being screened. Resonant frequencies of subsequently screened capacitors could then be compared with these population distributions to assess the likelihood of cracks being present. To explore the feasibility of such an approach, an analysis of the statistics of measured frequencies of cracked and uncracked MLCCs was conducted.

No cracks were optically detected in the AR specimens in any of the groups listed in Table I. After heat treatment, the majority of specimens were visibly cracked, including all of the specimens in Groups 2 – 7 and Group 9. Heat-treated specimens with no visible cracks included four in Group 1, all specimens in Groups 8, six in Group 10, and three in Group 11.

As described above, the two peaks near 600 kHz were simultaneously fit to a sum of two Pearson VII functions to reduce skewing of the fit to the main peak that would arise from the presence of the smaller instrumental peak if a single Pearson VII function were used. The frequencies of the RUS peaks near 460 kHz and 990 kHz were similarly determined by fitting to a sum of two Pearson VII functions.

Figures 6 and 7 show, for all the specimens in this study, the frequencies determined with the above fitting procedure for the three principal RUS peaks between 400 kHz and 1100 kHz. Spectra for MLCC Groups 9, 10 and 11 were acquired only over a frequency range near 990 kHz.

Before proceeding with an analysis of correlations of the frequencies with the presence of visible cracks, we consider whether the data show a significant dependence of the frequencies of the cracked MLCCs on the temperature of heat treatment. It would not be surprising, for example, to find that greater thermal shocking from higher heat-treatment temperatures leads to increases in the number and/or size of cracks and greater associated shifts in resonant frequencies. One-way Analyses of variance (ANOVAs) were performed on the frequency data for the visibly cracked HT specimens with the group number as a categorical index. The results of these analyses show that, based on a confidence interval with p = 0.05, differences in the means of the groups are not statistically significant. The p-values were 0.07, 0.39, and 0.68 for the peaks near 463 kHz, 584 kHz, and 990 kHz, respectively. Similar ANOVAs performed separately on the AR and HT capacitors without visible cracks found no statistically significant differences in mean frequencies of the groups. In the absence of significant evidence of a dependence of the frequency on heat-treatment temperature within each of the three categories, analyses of differences between these categories were pursued without heat-treatment temperature as a variable. In other words, all of the heat-treatment groups were considered as a single set within each of the three categories (AR, HT without cracks, and HT with cracks).

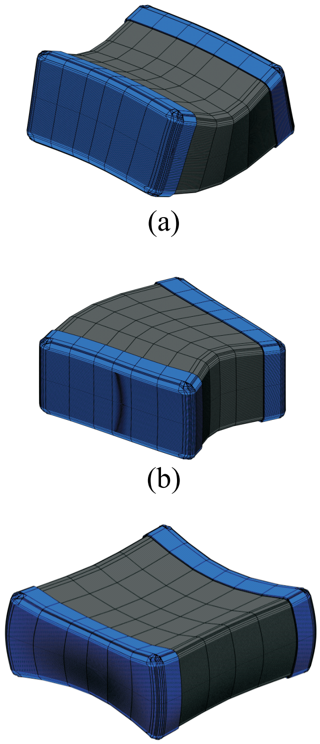

(a)

(b)

(c)

Fig. 5. Displacement patterns calculated from the FE model for modes at (a) 474 kHz, (b) 590 kHz, and (c) 970 kHz.

kHz, 970 kHz, and 977 kHz [19]. The calculated frequencies of 474 kHz, 590 kHz, and 977 kHz are, respectively, within 1.7 %, 1.3 %, and 1.4 % of the three strongest measured peaks in Fig. 3(a) at (465.8 +/- 1.1) kHz, (582.1 +/- 0.3) kHz, and (990.5 +/- 0.3) kHz (not including the peak near 600 kHz that is identified as an instrumental artifact). The corresponding calculated displacement patterns for these three modes are shown in Fig. 5. These patterns consist predominantly of (a) flexural displacements normal to the largest surface, (b) flexural displacements normal to the second largest surface, and (c) extensional displacements normal to the second largest surface, respectively.

Several additional weak peaks are also seen in the RUS spectra but are not visible on the linear scale of Fig. 4, and the frequencies of these peaks are consistent with those predicted from FE calculations for other modes [19]. The relatively small height of these peaks is understood to arise from the fact that the strength of acoustic excitation of a given mode is dependent on its symmetry and the contact configuration of the transducers.

B. Correlation of resonant frequencies with the presence of cracks

The central objective of this study is to assess whether a nondestructive screening technique can be developed to detect the presence of dielectric cracks in MLCCs through the use of resonant-frequency spectra. For such screening, data will

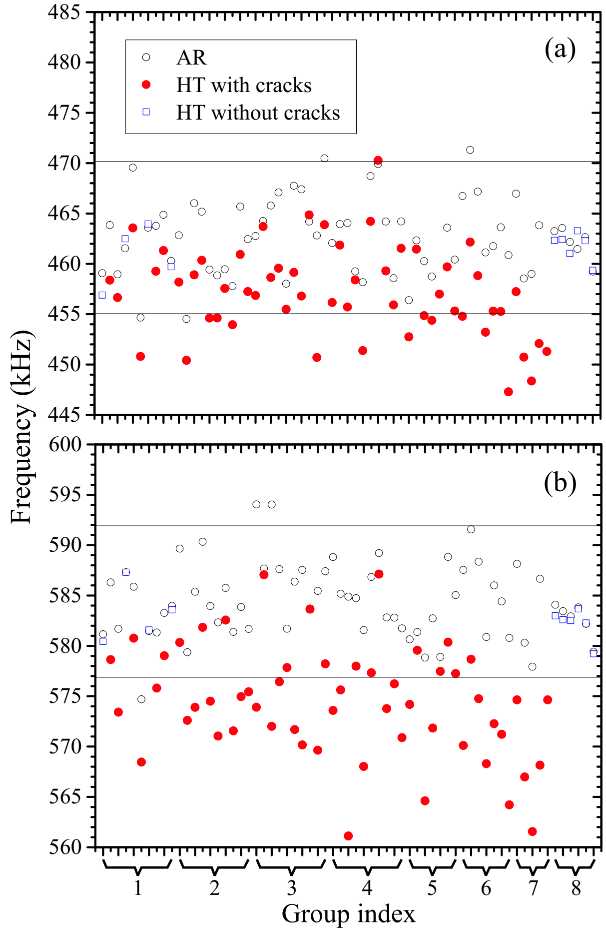

Fig. 6. Frequencies of RUS peaks near (a) 463 kHz and (b) 584 kHz before and after heat treatment. Horizontal lines in these graphs are at the frequencies that are two standard deviations below and above the mean of the measured frequencies of the as-received (AR) capacitors.

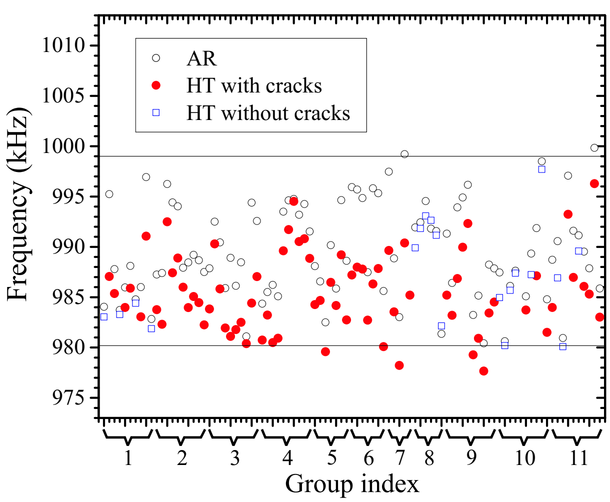

Fig. 7. Frequencies of RUS peaks near 990 kHz before and after heat treatment. Horizontal lines in these graphs are at the frequencies that are two standard deviations below and above the mean of the measured frequencies of the as-received (AR) capacitors.

Table II lists results of statistical analyses of the frequencies that are plotted in Figs. 6 and 7 for each of the three principal peaks. Shapiro-Wilk tests of normality of the frequencies were performed separately for each of the three MLCC categories (AR, HT with visible cracks, and HT without visible cracks) for each of the three modes. At the $p = 0.05$ confidence level, normality cannot be rejected for any of the data sets. In other words, the data for the peaks in each of the three frequency ranges are consistent with their having been drawn from a normally distributed population for each category.

For the two higher-frequency modes (near 584 kHz and 990 kHz in AR specimens), the scatter in the frequencies of the AR specimens is believed to be dominated by dimensional variations of the specimens. This conclusion is consistent with the fact that the fractional standard deviations of the three orthogonal dimensions were measured to be 0.27 % to 1.1 % (Sec. II) and the fractional standard deviations of the frequencies near 584 kHz and 990 kHz are in the middle of this range (0.6 % and 0.5 %, respectively). Many resonant frequencies of objects are approximately inversely proportional to some linear combination of dimensions. In the simple case of an isotropic sphere, for example, all resonant frequencies are exactly inversely proportional to the radius of the sphere [22].

The standard deviations associated with variations in transducer contact were found to be more than an order of magnitude smaller (0.3 kHz) than the corresponding values of σ listed in Table II for the two higher-frequency modes. Uncertainties in the individual fit frequencies for these modes (with the selected dual-Pearson function) were less than 0.01 % and, therefore, not a significant contribution to the AR standard deviations in Table II.

Dimensional variations are also believed to be the dominant factor contributing to the scatter in frequencies of the mode near 463 kHz in AR specimens. However, for this mode, the measured variations in frequency associated with variable transducer contact are only a factor of 3.5 times smaller than the value of σ for AR specimens in Table II. Therefore, this uncertainty contributes significantly to the standard deviation listed in this table.

ANOVAs performed with a categorical index corresponding to AR and HT showed that the mean frequency of HT specimens without visible cracks were, in each of the three frequency ranges, not significantly different from those of the AR specimens, based on a standard cutoff of 0.05 for the p-values (Table II). The mean frequencies of the three data sets of HT specimens with cracks were all found to be significantly different from those of the corresponding AR specimens (Table II).

For the case of normally distributed data sets, as in Table II, an alternate statistical approach for evaluating differences in mean values is the two-sample Z-test. The Z-value for two sets of measured frequencies is given by [23]

$$Z = \frac{\bar{f}_1 - \bar{f}_2}{(\sigma_1^2/N_1 + \sigma_2^2/N_2)^{1/2}}, \qquad (2)$$

TABLE II

STATISTICAL ANALYSIS OF FREQUENCIES f FOR THE THREE CONDITIONS OF MLCCS, INCLUDING MEAN, STANDARD DEVIATION, p-VALUE OF SHAPIRO-WILK NORMALITY TEST, p-VALUE OF ANOVA, TWO-SAMPLE Z-VALUE FOR THE HT DISTRIBUTION RELATIVE TO THE CORRESPONDING AR DISTRIBUTION, AND THE FRACTION OF THE HT DISTRIBUTION THAT LIES WITHIN $2\sigma_{\mathrm{AR}}$ OF THE CORRESPONDING AR MEAN.

MLCC condition	Mean f (kHz)	σ of f (kHz)	Number of specimens	Shapiro-Wilk p-value	ANOVA p-value	Z-value	Fraction within $2\sigma_{\mathrm{AR}}$ of AR mean
AR	462.62	3.78	64	0.66			0.95
	584.02	3.33	64	0.62			0.95
	989.56	4.71	93	0.09			0.95
HT without cracks	461.37	2.15	10	0.90	0.31	1.5	1.00
	582.61	2.15	10	0.44	0.57	1.8	0.99
	987.00	4.86	19	0.40	0.07	2.1	0.91
HT with cracks	457.15	4.53	55	0.23	0.00	7.1	0.67
	574.32	5.58	55	0.89	0.00	11.3	0.29
	985.49	3.93	75	0.63	0.00	6.1	0.91

where $\bar{f}_1$ and $\bar{f}_2$ are the mean frequencies, σ_1 and σ_2 are the standard deviations, and N_1 and N_2 are the number of data values in each data set. The second-to-last column in Table II lists the Z-values for each of the HT data sets relative to the corresponding AR data set. Following the common interpretation of results from a Z-test, Z-values less than 2.0 indicate that there is no statistically significant evidence of a difference in the means of the two populations from which the data were drawn, and Z-values greater than 2.5 are consistent with the means being significantly different. Therefore, the Z-values listed in Table II for the HT specimens without visible cracks provide no significant evidence that the mean frequencies of the distributions for the modes near 463 kHz or 584 kHz are different than the corresponding means of the distributions for the AR data sets. The Z-value of 2.1 for the mode with frequencies near 987 kHz provides marginally significant evidence for this distribution being different than the AR distribution. The Z-values of all three of the data sets for the HT specimens with visible cracks (7.1, 11.3, and 6.1) provide highly significant evidence for the means being different than the corresponding means for the AR specimens. These results are similar to those obtained from the ANOVAs on the raw data (not involving the Gaussian fit parameters), including the fact that the ANOVA p-value for the data from the HT specimens with frequencies near 987 kHz is close to the nominal cutoff of 0.05 (Table II). From the Z-test, the statistically strongest evidence for a difference in the means of the underlying populations of the cracked HT specimens and AR specimens is obtained for the mode with a mean frequency near 574 kHz in cracked specimens.

The last column in Table II lists the fraction of the fit normal distributions (specified by the means and standard deviations) that lie within $2\sigma_{\mathrm{AR}}$ of the corresponding AR mean frequency (specified by values in the first three rows of the table). By definition, the fraction of the AR distributions within these ranges is 0.95 (i.e., 95 % of the AR distributions are within two standard deviations of the mean). The values in the last column for the HT specimens with visible cracks show that 91 % to 100 % of the fit distributions for these specimens lie within $2\sigma_{\mathrm{AR}}$ of the corresponding AR mean for each mode. For the HT specimens with visible cracks, 67 %, 29 %, and 91 % of the fit distributions of frequencies for the lower, middle, and higher peaks, respectively, are within $2\sigma_{\mathrm{AR}}$ of the corresponding AR mean.

V. DISCUSSION

The results in the last two columns of Table II suggest that, with the RUS approach, measurements of the frequency of the dominant mode near 584 kHz provide the most promising basis for nondestructively detecting the presence of cracks in MLCCs of the type studied here. With the $\pm\ 2\sigma_{\mathrm{AR}}$ range of the AR frequency distribution employed as a criterion for acceptance/rejection, the results for this mode indicate that approximately 71 % of cracked MLCCs would be rejected.

In two previously published studies [13], [14], we explored the correlation of measurements of acoustic nonlinearity with the presence of visible cracks in MLCCs with the same nominal specifications and manufacturing parameters and similar heat treatments as those employed in the current study. Unlike the data in the current study, Shapiro-Wilk tests of normality of the measured nonlinearity parameters showed that these data were not consistent, after heat treatment, with a Gaussian distribution, although they were consistent with a Gaussian distribution before heat treatment. Therefore, rather than look at the overlap of fit distributions to assess the shifts in the HT data relative to the AR data in those studies, the analysis involved simply counting the number of HT specimens that had nonlinear parameters outside of a specified range of the fit AR distribution. In our first nonlinear study of these MLCCs [13], analysis of correlations of the presence of cracks was pursued by counting the numbers of MLCCs with and without cracks that had nonlinear parameters within and outside of a range of two standard deviations ($2\sigma_{\mathrm{AR}}$) of the AR mean. This led to a rejection rate of 89 % for cracked HT specimens. In the second nonlinear study on the same specimens, we performed time-domain nonlinear-acoustic analysis of resonant ringdown to determine nonlinear parameters and found a rejection rate of approximately 93 % with a $\pm\ 3\sigma_{\mathrm{AR}}$ criterion that included 99.7 % of the AR distribution.

A comparison of the dominant-mode rejection rate of 71 % found for cracked samples in the current study and the rejection rates described above from the previous nonlinear studies supports the conclusion that nonlinear elastic properties are more strongly correlated with the presence of cracks in type-1210 MLCCs than are linear elastic properties (which determine resonant frequencies in conventional RUS). However, in considering approaches for industrial screening of MLCCs, it is useful to note that RUS offers potential advantages for less-critical applications, with respect to simplicity of hardware implementation and analysis of measurements. The narrow-band excitation of RUS also may provide substantial advantages in situations where interference of spurious modes makes nonlinear tone-burst measurements impractical. In particular, it would not be surprising to find that spurious mode interference will be a substantial issue in any future testing of MLCCs mounted to circuit boards, since acoustic coupling to a board is likely to lead to excitation of additional acoustic modes. In such a situation, broader-band tone-burst techniques will simultaneously excite any nearby spurious modes, and analysis of signals to extract nonlinear parameters could be intractable. In contrast, RUS spectra with overlapping peaks can be analyzed by fitting with functions that include multiple peaks, as used in this study.

VI. Conclusion

The results presented here demonstrate that RUS is a promising approach for screening MLCCs for cracks that cannot be detected through electrical measurements before service and can lead to eventual device failure. Among three resonant modes excited most strongly in type-1210 MLCCs with the selected RUS transducer configuration, the dominant mode (near 584 kHz in as-received specimens) was found to be most sensitive to the presence of visible surface-breaking cracks. Analysis of Gaussian fits to the measured frequency distributions of this mode showed that heat-treated specimens without visible cracks had a distribution that was not significantly different from that of the as-received specimens, while the distribution for specimens with cracks was shifted significantly downwards. A criterion for acceptance/rejection based on a symmetric frequency range spanning 95 % of the distribution for the as-received specimens ($\pm$ two standard deviations) led to 71 % of the distribution for the visibly cracked specimens being rejected. This rejection percentage is less than those previously reported in two previous nonlinear-acoustic studies of similar MLCCs [13], [14], which suggests that linear acoustic measurements are less sensitive than nonlinear measurements to the presence of cracks in this type of capacitor. Nevertheless, the relative simplicity of RUS makes it a potentially attractive choice for enhanced screening of MLCCs in applications that do not require optimal reliability. The narrow-band excitation employed in RUS would also provide advantages over tone-burst techniques in situations where spurious modes substantially interfere with measurements of the resonant modes of interest.

VII. Acknowledgement

The authors are grateful to Alexander Teverovsky for useful discussions on failure and characterization of MLCCs.

References

[1] M. Keimasi. "Flex cracking and temperature-humidity-bias effects on reliability of multilayer ceramic capacitors," University of Maryland, Mechanical Engineering Department, PhD Dissertation (2007).

[2] A. Teverovsky, "Effect of manual-soldering-induced stresses on ceramic capacitors (Part I)," NASA/NEPP Task Report (2008).

[3] G. Brock, "Reliability of multilayer ceramic capacitors," University of Maryland, Mechanical Engineering Department, Masters Thesis (2009).

[4] N. Blattau and C. Hillman, "Design guidelines for ceramic capacitors attached with SAC solder," *Proceedings IPC APEX EXPO 2006* (Anaheim, CA, February 7-10, 2006).

[5] D. S. Erdahl and I. C. Ume, "Online-offline laser ultrasonic quality inspection tool for multilayer ceramic capacitors - Part I," *IEEE T. Adv. Pack.*, 27 (2004) pp. 647-653; *IEEE Trans. Adv. Pack.*, 28 (2005) pp. 264-272.

[6] D. S. Erdahl and I. C. Ume, "Online-offline laser ultrasonic quality inspection tool for multilayer ceramic capacitors - Part II," *IEEE Trans. Adv. Pack.*, 28 (2005) pp. 264–272.

[7] O. Boser, P. Kellawon, and R. Geyer, "Electromechanical resonances in ceramic capacitors and their use for rapid nondestructive testing," *J. Am. Ceram. Soc.*, 72 (1989) pp. 2282-2286.

[8] J. Pritchard, C. R. Bowen, and F. Lowrie, "Multilayer actuators: Review," *Brit. Ceram. T.*, 100 (2001) pp. 265-273.

[9] K. Prume, R. Waser, K. Franken, and H. R. Maier, "Finite-element analysis of ceramic multilayer capacitors: Modeling and electrical impedance Spectroscopy for a nondestructive failure test," *J. Am. Ceram. Soc.* 83, 1153 1159 (2000).

[10] A. D. Kostic and S. W. Schwartz, "Optimized acoustic microscopy screening for multilayer ceramic capacitors," *Proceedings of the IEEE Reliability and Maintainability Symposium 2011*, pp. 1–4.

[11] S. A. Kim, W. L. Johnson, G. S. White, and R. Roberts, "Ultrasonic detection of defects in multilayered ceramic capacitors for active implantable medical devices," *Proceedings of Materials and Processes for Medical Devices 2011* (Minneapolis, August 8-10, 2011), pp. 80–85 (2013).

[12] W. L. Johnson, S.A. Kim, T.P. Quinn, and G.S. White, "Nonlinear acoustic effects in multilayer ceramic capacitors," in *Review of Progress in Quantitative Nondestructive Evaluation: Vol. 32* (AIP Conference Proceedings, Vol. 1511) (AIP, Melville, 2013) pp. 1462-1469.

[13] W. L. Johnson, S. A. Kim, G. S White, and J. Herzberger, "Nonlinear resonant acoustic detection of cracks in multilayer ceramic capacitors," *Proceedings of the 2014 IEEE International Ultrasonics Symp.*, 244–247 (2014).

[14] W. L. Johnson, S. A. Kim, G. S. White, J. Herzberger, K. L. Peterson, and P. R. Heyliger, "Time-domain analysis of resonant acoustic nonlinearity arising from cracks in multilayer ceramic capacitors," in *4nd Annual Review of Progress in Quantitative Nondestructive Evaluation* (AIP Conference Proceedings, Vol. 1706) (AIP, Melville, 2016) 060005.

[15] A. Migliori, *Resonant Ultrasound Spectroscopy* (Johns Wiley and Sons, New York, 1997).

[16] B. J. Zadler and J. A. Scales, "Monitoring crack-induced changes in elasticity with resonant spectroscopy," *J. Appl. Phys.*, 104, 023536 (2008).

[17] G. Burns, P. Yang, *Vicinal light inspection of translucent materials*, US Patent, US7650028 B1 (2010).

[18] J. N. Reddy, *An Introduction to the Finite Element Method, 3rd edition* (McGraw-Hill, New York,NY, 2005).

[19] K. L. Peterson, W. L. Johnson, S. A. Kim, and P. R. Heyliger, "Vibrational modes of multilayered ceramic capacitors," *Finite Elem. Anal. Des.*, 116, 1-11 (2016).

[20] J. F. Cornwell, *Group Theory in Physics, Vol. I* (Academic, New York, 1984).

[21] K. Pearson "Mathematical contributions to the theory of evolution, XIX: Second supplement to a memoir on skew variation," *Philosophical Transactions of the Royal Society of London*, A 216, 429457 (1916)

[22] Y. Sato and T. Usami, "Basic study of the oscillation of a homogeneous elastic sphere, I. Frequency of the free oscillation," *Geophys. Mag.*, 31, 15–24 (1962).

[23] D. Freedman, R. Pisani, and R. Purves, *Statistics, 4th Edition* (W. W. Norton and Company, New York, NY, 2007).